https://doi.org/10.5194/wes-2026-76
Preprint. Discussion started: 13 May 2026

eawe european academy of wind energy
Open Access WIND ENERGY SCIENCE DISCUSSIONS

A generalised Gaussian wake model based on extended actuator disc theory

Zheni Fei[1], Takafumi Nishino[1], and Christopher R. Vogel[1]
[1]Department of Engineering Science, University of Oxford
Correspondence: Zheni Fei (zheni.fei@eng.ox.ac.uk)

Abstract. Engineering wake models have been widely used for wind farm design and optimization due to low computational cost. Recent work suggests that the key to improving the wake models lies in the prediction of the transition point between the 'near-wake' and 'far-wake' regions. This study proposes an analytical model for this transition point based on a relationship between the wake-centreline pressure gradient and the divergence of Reynolds shear stresses. Using this relationship together with an extended actuator disc analysis for a turbine in a laterally confined flow, the proposed model also predicts the initial wake profile at the start of the far-wake region for any practical inflow turbulence conditions and local blockage ratios. In addition, a new Gaussian far-wake model considering the local blockage effect is formulated to form a complete engineering wake model. The model is validated against a series of Reynolds-averaged Navier-Stokes (RANS) simulations of an actuator disc over a wide range of inflow turbulence intensities, thrust coefficients and local blockage ratios. The model predictions are in good agreement with the simulation results.

1 Introduction

Wind energy is a significant source of renewable energy. Growing demand has led to the deployment of larger wind turbines as well as larger and denser wind farms, making the prediction of turbine wakes more and more important. Analytical wake models are often used for farm design and planning due to their reasonable accuracy and low computational cost. However, existing wake models still have difficulties with various real-world flow conditions, such as those observed in a large wind farm.

The wake of a turbine is often divided into a far-wake region, which is dominated by the Reynolds shear stresses, and a near-wake region, which is affected by both the pressure gradient and the Reynolds shear stresses. Most existing wake models have been derived to predict the development of the far wake. The classical models assume top-hat (Jensen, 1983; Frandsen et al., 2006) or Gaussian (Bastankhah and Porté-Agel, 2014) wake profiles. Some models consider only mass conservation within the wake (Jensen, 1983); however, more recent examples also consider momentum conservation within the wake (Frandsen et al., 2006; Bastankhah and Porté-Agel, 2014). Recent models (Shapiro et al., 2019; Blondel and Cathelain, 2020; Qian and Ishihara, 2018; Niayifar and Porté-Agel, 2016) descend from these classical ones and focus on improving the relationship between the wake expansion rate and the turbulence intensity. However, these models only consider the reduction in flow speed within the wake and ignore the increased speed of the flow bypassing the turbine and the resulting pressure variation; thus, they do not

https://doi.org/10.5194/wes-2026-76
Preprint. Discussion started: 13 May 2026

eawe european academy of wind energy
Open Access WIND ENERGY SCIENCE DISCUSSIONS

truly conserve mass and momentum in a control volume spanning from far upstream to far downstream of the turbine. Some models try to include more physical processes to describe the correct wake recovery; for example, those based on diffusion (Vahidi and Porté-Agel, 2022b), mass entrainment (Luzzatto-Fegiz, 2018) and solving an axisymmetric Reynolds-averaged Navier-Stokes (RANS) equation in polar coordinates (Ainslie, 1988). Although these models can capture the recovery rate of the far-wake region well, they still have difficulties in predicting the magnitude of the far-wake velocity accurately.

Recent work by Neunaber et al. (2024) suggests that the difficulty comes from uncertainty about near-wake conditions. They compared various wake models and showed that most models could predict the rate of far-wake recovery well and that the main discrepancy came from the near-wake length scale. After applying a data-fitted 'virtual origin', the location of a point source that can produce the same far wake of an actual drag body, the tested models almost collapsed onto a single curve and agreed much better with the experimental data. The importance of such a length scale was also discussed by Vahidi and Porté-Agel (2022a). They argue that since self-similarity also exists in the axial direction, there should be a length scale that can collapse the streamwise variations of centreline velocity for different turbulence cases onto a single curve. They also suggested that this length scale is the near-wake length and that it can be used to improve the generality of wake models. Thus, a robust and accurate near-wake model is crucial for future improvement of wake models.

Compared to far-wake modelling, the work to date on near-wake modelling is relatively limited due to its complexity and dependency on the details of turbine design and operation. In addition to the conventionally-assumed near-wake length of two rotor diameters, Vahidi and Porté-Agel (2022a) discussed three near-wake length models. The earliest one is a semi-empirical model based on experimental data (Vermeulen, 1980), and is modified from Lissaman (1979)'s classical model. Abramovich et al. (1984) based his model on turbulent jet theory, and was one of the earliest models to model the end of the near wake and the start of the far wake separately. Models for the near wake length have been developed based on vortex stability, e.g. Sørensen et al. (2014). However, the near-wake length alone is not sufficient to parametrise the input to the far wake; the velocity deficit is also needed as implied by the idea of virtual origin argued by Neunaber et al. (2024).

Conventionally, the initial velocity far wake deficit is taken to be $2a$ for a single turbine, where a is the axial induction factor at the rotor plane, based on the classical actuator disc model for a turbine in a uniform inviscid flow. Since the near-wake velocity deficit is likely to change with turbulence conditions, Ainslie (1988) adopted an empirical formulation based on wind tunnel data measured at two rotor diameters downstream of the turbine. This formulation only considers the effect of turbulence, which may not be sufficient for large turbines in a wind farm. When the turbines are placed in a farm and when there is a low atmospheric inversion layer, the local blockage effect (Nishino and Draper, 2015) can change the relationship between the axial induction factor and the near-wake centreline velocity. Garrett and Cummins (2007) provided an analytical solution for the velocities in the wake and bypass flows under the local blockage effect. However, their method assumes an inviscid flow with a top-hat wake profile. These assumptions are contradictory to the assumptions usually made for the start of the far wake, where the wake profile is Gaussian, which means that turbulent mixing in the near-wake region needs to be additionally considered (Nishino and Willden, 2013).

To resolve the above challenges, this study derives an analytical solution to the near-wake length and the corresponding wake deficit for given inflow turbulence intensities, thrust coefficients and local blockage ratios. Under the assumption of a

https://doi.org/10.5194/wes-2026-76
Preprint. Discussion started: 13 May 2026

eawe european academy of wind energy
Open Access WIND ENERGY SCIENCE DISCUSSIONS

self-similar Gaussian wake, the only input parameters required are the turbulence intensity and the mixing length of the inflow (used to model the Reynolds shear stresses), turbine thrust coefficient, turbine diameter, freestream velocity and the local blockage ratio. The idea of modelling the centreline Reynolds shear stresses using the eddy viscosity hypothesis follows the wake model derived by Anderson (2009), who simplified Ainslie (1988)'s model by assuming a self-similar Gaussian wake profile.

The paper is organised as follows. Section II briefly introduces the RANS simulations conducted to verify the analytical model, Section III describes the physical concept of the analytical model and presents how the model is formulated, and then Section IV compares the model prediction against the simulation results and other wake models to discuss the important modelling elements. Section V summarises what has been achieved by the new model and how it can be developed further.

2 Numerical simulations

Three-dimensional Reynolds-averaged Navier-Stokes (RANS) simulations with a modified k-ϵ turbulence model have been performed using OpenFOAM to verify the proposed wake model. The RANS actuator disc code is adapted from the original code by Svenning (2010) which has been validated by the data from Mikkelsen (2003).

To specify the turbulence level experienced by the turbine, we add a pair of source terms to the standard k-ϵ turbulence model to ensure that the turbulence does not decay. The k-ϵ model in OpenFOAM solves

$$\frac{D}{Dt}(\rho k) = \nabla \cdot (\rho D_k \nabla k) + P_k - \rho\epsilon + S_k \tag{1}$$

and

$$\frac{D}{Dt}(\rho \epsilon) = \nabla \cdot (\rho D_\epsilon \nabla \epsilon) + \frac{C_1 \epsilon}{k}(P_k + C_3 \frac{2}{3} k \nabla \cdot \boldsymbol{u}) - C_2 \rho \frac{\epsilon^2}{k} + S_\epsilon, \tag{2}$$

where k is turbulent kinetic energy, t is time, D_k is the eddy diffusivity for k, P_k is the turbulent kinetic energy production rate, S_k is the internal source term for k, ϵ is the turbulent kinetic energy dissipation rate, D_ϵ is the effective diffusivity for ϵ, C_1, C_2 and C_3 are all model coefficients, $\boldsymbol{u}$ is the velocity vector, and S_ϵ is the internal source term for ϵ. For the standard implementation of the $k-\epsilon$ model, both S_k and S_ϵ equal zero. In this study, we used the 'scalarSemiImplicitSource' function in OpenFOAM to add the source terms, so that the turbulence does not decay in uniform flow. The two source terms are

$$S_k = \rho\epsilon \tag{3}$$

and

$$S_\epsilon = C_2 \rho \frac{\epsilon^2}{k}. \tag{4}$$

By substituting Eq. (3) and (4) into Eq. (1) and (2) respectively, we can show that when the flow is uniform, both k and ϵ do not decay and remain constant. The same approach was previously used by Van der Laan et al. (2015).

The turbine is represented as a disc, 40 m in diameter and 1 m in thickness, placed $15D$ downstream from the inlet and $25D$ upstream from the outlet of a rectangular computational domain, where D is the disc diameter. A volume force was uniformly

https://doi.org/10.5194/wes-2026-76
Preprint. Discussion started: 13 May 2026

eawe european academy of wind energy
Open Access WIND ENERGY SCIENCE DISCUSSIONS

distributed within the disc. No hub or support structure is simulated and the tangential force is turned off to yield the simplest case of the disc reducing only the axial momentum of the flow.

For all the cases simulated, the uniform incoming flow speed U_0 is 10 m/s. The Reynolds number, defined as $Re = \frac{U_0 D}{\nu} = 2.67 \times 10^7$, where ν is the kinematic viscosity set to be 1.5×10^{-5} m^2/s. The mixing length l at the inflow is 10 m. A range of inflow turbulence intensities, thrust coefficients and blockage ratios are simulated and summarised in Table 1, where Ti is the inflow turbulence intensity, B is the blockage ratio defined as A_d/A_c, A_d is the disc area, A_c is the cross-sectional domain area, C_t is the thrust coefficient defined as $T/0.5\rho U_0^2 A_d$, T is the thrust exerted by the disc, ρ is the fluid density. In the rest of the paper, unless otherwise stated, the flow conditions of each case follow $B = 0.1\%$, $Ti = 10\%$, and $C_t = 0.6259$. The boundary conditions are summarised in Table 2. The inlet k is calculated from Ti as $1.5(TiU_0)^2$, and the corresponding inlet ϵ is calculated as $C_\mu^{0.75} k^{1.5}/l$, where C_μ is a model constant equal to 0.09. The turbulent eddy viscosity is calculated in the same way as that in a standard k-ϵ model, which is

$$\nu_t = C_\mu \frac{k^2}{\epsilon}. \tag{5}$$

Table 1. Summary of flow parameters for the RANS simulations.

	cases 1-4	cases 5-8	cases 9-11
$Ti(\%)$	10	1 5 10 20	10
B (%)	1 5 10 20	0.1	0.1
C_t	0.6259	0.6259	0.36 0.75 0.8889

Table 2. Summary of boundary conditions for the RANS simulations.

	Inlet	Outlet	Sidewalls
U	fixed value	zero gradient	slip
p	zero gradient	fixed value	zero gradient
k and ϵ	fixed value	zero gradient	zero gradient

https://doi.org/10.5194/wes-2026-76
Preprint. Discussion started: 13 May 2026

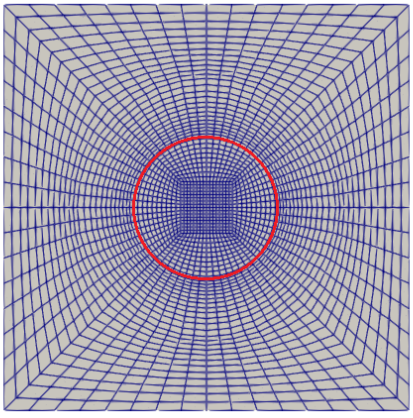

Figure 1. Cross-sectional view of the level 1 mesh for $B = 10\%$. The red circle indicates the disc location.

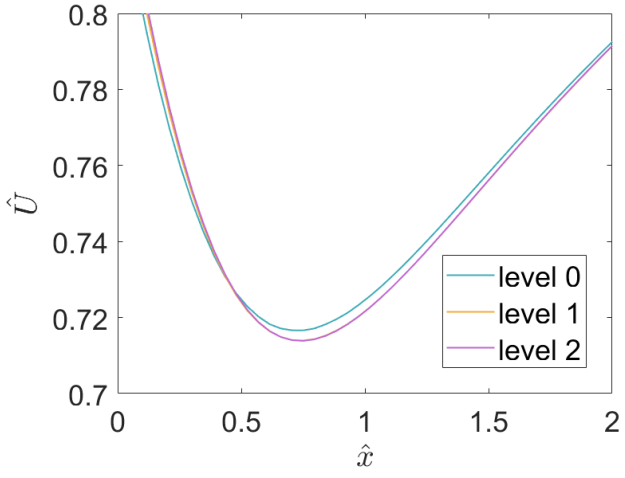

Figure 2. Comparison of streamwise velocity and velocity gradient profiles along the wake centreline (for $B = 10\%$) demonstrating the mesh convergence.

The 'blockmesh' function in OpenFOAM was used to generate multi-block structured grids with hexahedral cells. A cross-sectional view of the final mesh for $B = 10\%$ is shown in Fig. 1. The red circle outlines the location and size of the actuator
105 disc, which has an O-type structured mesh. Outside of the disc region, an axisymetrical mesh structure was used to capture the wake accurately. For other blockage ratio cases, the mesh within this circular region remains unchanged. Only the mesh between the wake circle and the square domain is adjusted to different domain sizes.

In the streamwise direction, the mesh is refined near the disc and expands in the downstream direction. The disc region is meshed independently, and the actual disc ($0.025D$ thick) is located in the middle of the disc region ($0.03D$ thick). The mesh

https://doi.org/10.5194/wes-2026-76
Preprint. Discussion started: 13 May 2026

eawe european academy of wind energy
Open Access WIND ENERGY SCIENCE DISCUSSIONS

in this region is very fine (with 12 cells being uniformly distributed across the $0.03D$-thick region) to ensure that the volume force exerted on the domain is accurate and does not change in the mesh convergence study.

This baseline mesh is refined using the 'SnappyHexMesh' function in OpenFOAM to obtain three additional meshes for a mesh convergence study. The refinement level is defined such that level n divides each cell in the baseline mesh into 2^n parts in each direction. The results of the convergence study are shown in Fig. 2, demonstrating that the solutions for levels 1 and 2 are almost the same. As a compromise between accuracy and computational cost, refinement level 1 is adopted in this study. The final mesh (for $B = 10\%$) consists of 988608 hexahedral cells. The sizes of the cells near the disc are $0.05D$ in the tangential direction and $0.021D$ in the radial direction.

3 Analytical model

We consider a single turbine represented by an actuator disc placed in a confined flow passage with a cross-sectional area A_c as shown in Fig. 3. The vertical black solid line denotes the actuator disc. The green lines outline the streamtube for conventional actuator disc analysis, where the pressure is assumed to be uniform within the streamtube at each streamwise position. The present model is developed considering an infinitesimally thin streamtube located along the wake centreline, denoted with orange lines in the figure. The yellow dashed lines depict the wake boundary defined by the position where the streamwise velocity is 99% of the freestream velocity. Outside the wake boundary, the velocity is assumed to be uniform, which we refer to as the bypass velocity.

For the sake of convenience, we define five stages of the flow. Stage 1 is far upstream of the turbine before the induction starts. Both static pressure p_0 and the velocity U_0 are uniform across the entire cross-section and are equal to the freestream condition. The cross-sectional area of the centreline streamtube is δA_1. Stage 2 is at the turbine disc position. Within the streamtube across the turbine disc, the static pressure is p_2^+ immediately upstream of the disc and p_2^- immediately downstream of the disc. The velocity within the centreline streamtube is U_2 at the disc, and the cross-sectional area of the centreline streamtube is δA_D. Stage 3 is located downstream of the turbine at the start of the far wake. The static pressure is assumed to be uniform across the entire cross-section and is equal to p_3. The velocity is U_3 within the centreline streamtube and U_{3b} outside the wake boundary. The cross-sectional area of the centreline streamtube is δA_3. Stage 4 encompasses the far wake region where most of the wake recovery happens. Stage 5 is the location where the flow is considered to be fully evolved with uniform velocity U_0 and the static pressure recovers to $p_5 \leq p_0$. The origin of the coordinate system considered in this model is placed at the disc centre.

It is assumed that the flow is steady, and the mean velocity of the far wake is axisymmetrical, self-similar, and has a Gaussian profile, which has the form of

$$\frac{U}{U_0} = \beta - Ce^{-\frac{y^2+z^2}{2\sigma^2}}, \tag{6}$$

where U is the streamwise velocity component of the mean flow, y and z are spanwise and vertical coordinates, σ is the standard deviation of the Gaussian profile (also referred to as wake characteristic width), β is the bypass velocity normalised

https://doi.org/10.5194/wes-2026-76
Preprint. Discussion started: 13 May 2026

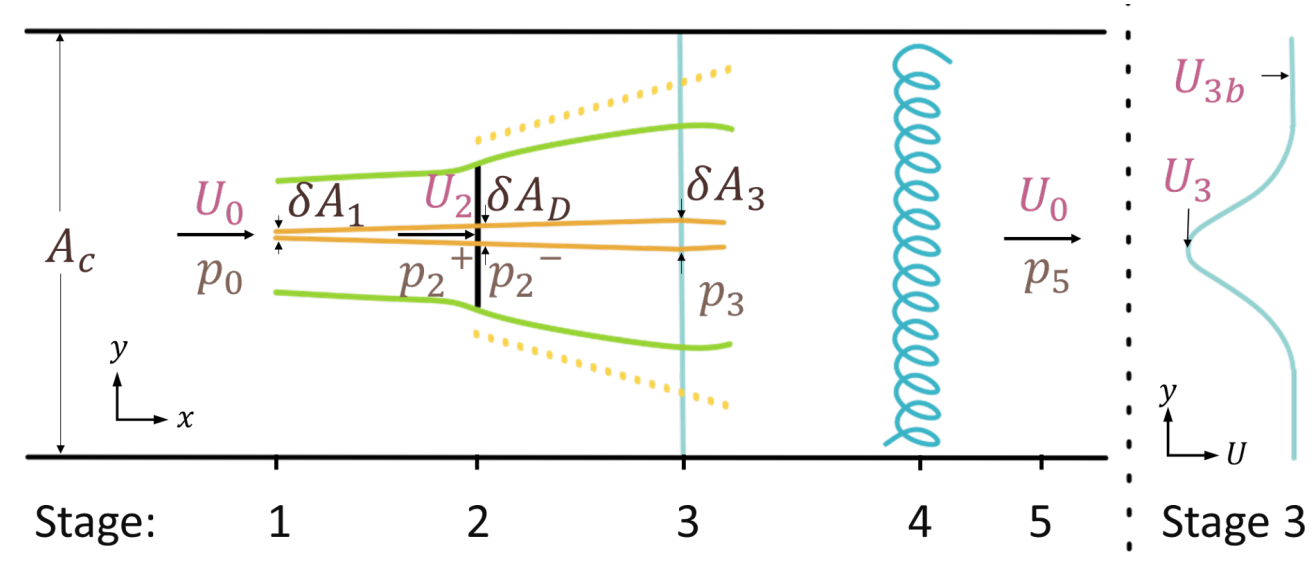

Figure 3. Schematic of the flow field around an actuator disc (left) and the wake velocity profile at the start of the far wake (right).

by the freestream velocity, and C is the normalised centreline velocity deficit defined as

$$C = \beta - \alpha, \tag{7}$$

where α is the centreline velocity normalised by the freestream velocity. Note that α, β and σ change with the streamwise position x. In the following subsections, we describe how these three parameters are calculated for Stages 3 and 4, as well as the streamwise position of Stage 3 (from which position the far-wake model is applicable).

3.1 Wake centreline momentum and energy balance

To solve the wake profile, we need three equations to find the three variables: α, β and σ. These equations can be derived from the conservation of energy, mass and momentum. We start by examining the streamwise component of the RANS equations given as

$$U\frac{\partial U}{\partial x} + V\frac{\partial U}{\partial y} + W\frac{\partial U}{\partial z} = -\frac{1}{\rho}\frac{\partial p}{\partial x} + \nu\left(\frac{\partial^2 U}{\partial x^2} + \frac{\partial^2 U}{\partial y^2} + \frac{\partial^2 U}{\partial z^2}\right) - \frac{\partial \overline{u'u'}}{\partial x} - \frac{\partial \overline{u'v'}}{\partial y} - \frac{\partial \overline{u'w'}}{\partial z}, \tag{8}$$

where V and W are spanwise (y) and vertical (z) mean velocities, respectively, p is static pressure, and $\overline{u'u'}$, $\overline{u'v'}$, $\overline{u'w'}$ are the streamwise, spanwise and vertical components of the Reynolds stresses, respectively. We then use the Boussinesq (linear) eddy viscosity hypothesis which states

$$\overline{u'u'} = \frac{2}{3}k - 2\nu_t\frac{\partial U}{\partial x},\quad \overline{u'v'} = -\nu_t\left(\frac{\partial U}{\partial y} + \frac{\partial V}{\partial x}\right),\quad \overline{u'w'} = -\nu_t\left(\frac{\partial U}{\partial z} + \frac{\partial W}{\partial x}\right), \tag{9}$$

where ν_t is the eddy viscosity. Along the centreline in the near-wake region, $V\frac{\partial U}{\partial y} = W\frac{\partial U}{\partial z} = 0$ due to symmetry, ν is much smaller than ν_t, and we assume that $\frac{\partial \overline{u'u'}}{\partial x}$, $\nu_t\frac{\partial^2 V}{\partial x \partial y}$ and $\nu_t\frac{\partial^2 W}{\partial x \partial z}$ are negligibly small compared to other remaining terms.

https://doi.org/10.5194/wes-2026-76
Preprint. Discussion started: 13 May 2026

eawe european academy of wind energy
Open Access WIND ENERGY SCIENCE DISCUSSIONS

Therefore, Eq. (8) for the wake centreline can be reduced to

$$U\frac{\partial U}{\partial x} = -\frac{1}{\rho}\frac{\partial p}{\partial x} + \nu_t\left(\frac{\partial^2 U}{\partial y^2} + \frac{\partial^2 U}{\partial z^2}\right). \tag{10}$$

In dimensionless form, it can be written as

$$\hat{U}\frac{\partial \hat{U}}{\partial \hat{x}} = -\frac{\partial \hat{p}}{\partial \hat{x}} + \hat{\nu}_t\left(\frac{\partial^2 \hat{U}}{\partial \hat{y}^2} + \frac{\partial^2 \hat{U}}{\partial \hat{z}^2}\right), \tag{11}$$

where $\hat{U} = U/U_0$, $\hat{p} = p/(\rho U_0^2)$, $\hat{\nu}_t = \nu_t/(U_0 D)$, $\hat{x} = x/D$, $\hat{y} = y/D$, and $\hat{z} = z/D$. We then define

$$\mathcal{R} = \hat{\nu}_t\left(\frac{\partial^2 \hat{U}}{\partial \hat{y}^2} + \frac{\partial^2 \hat{U}}{\partial \hat{z}^2}\right) \tag{12}$$

for convenience. Equation (11) suggests that the pressure gradient and the divergence of the Reynolds shear stresses ($\mathcal{R}$) are responsible for the variation of the centreline velocity. We integrate Eq. (11) along the wake centreline from upstream to the disc position and from the disc position to the position of interest in the wake, which gives

$$\frac{1}{2}(\alpha_2^2 - 1) = -(\hat{p}_2^+ - \hat{p}_0) + \int_{-\infty}^{\hat{x}_2} \mathcal{R}\, d\xi \tag{13}$$

and

$$\frac{1}{2}(\alpha^2 - \alpha_2^2) = -(\hat{p} - \hat{p}_2^-) + \int_{\hat{x}_2}^{\hat{x}} \mathcal{R}\, d\xi, \tag{14}$$

where the suffix 2 indicates that the variable is taken at Stage 2, and ξ is the dummy variable used to integrate with respect to the streamwise direction. We add Eq. (13) and (14) together, which gives

$$\frac{1}{2}(\alpha^2 - 1) = (\hat{p}_0 - \hat{p}) - (\hat{p}_2^+ - \hat{p}_2^-) + \int_{-\infty}^{\hat{x}} \mathcal{R}\, d\xi. \tag{15}$$

We assume the pressure is equalised between the wake and the bypass flow, before Stage 3 and is uniform in the spanwise direction at any location in the far-wake region, so we can calculate $\hat{p}$ by considering the Bernoulli equation in the bypass region, which is

$$\hat{p}_0 + \frac{1}{2} = \hat{p} + \frac{1}{2}\beta^2. \tag{16}$$

We add Eq. (16) and (15) and rearrange, which gives

$$\hat{p}_2^+ - \hat{p}_2^- = \frac{T}{\rho U_0^2 A_D} = \frac{1}{2}(\beta^2 - \alpha^2) + \int_{-\infty}^{\hat{x}} \mathcal{R}\, d\xi. \tag{17}$$

https://doi.org/10.5194/wes-2026-76
Preprint. Discussion started: 13 May 2026

eawe european academy of wind energy
Open Access WIND ENERGY SCIENCE DISCUSSIONS

Equation (17) describes the energy budget along the wake centreline. To solve for the wake profile, we still need two more equations. We use the continuity equation

$$\int_{A_c} U dA = U_0 A_c, \tag{18}$$

and the momentum deficit equation

$$\int_{A_c} U(U_0 - U) dA = \frac{T}{\rho} - \frac{(p_0 - p)A_c}{\rho}. \tag{19}$$

Recall the wake profile along the spanwise direction is defined by three variables, α, β and σ. Equations (17), (18) and (19) provide sufficient constraints to close the system if $\int_{-\infty}^{\hat{x}} \mathcal{R} d\xi$ is known.

3.2 Near wake velocity profile

Since we are mainly interested in the far wake, we aim to solve the velocity at Stage 3, which is the start of the far wake, and solve the rest of the far wake region using a marching approach. Thus, we need to find $\int_{-\infty}^{\hat{x}_3} \mathcal{R} d\xi$, and hence a more rigorous definition for Stage 3.

We start by studying the main driving forces in the near-wake region and how the centreline velocity varies. Figure 4 shows how the centreline velocity deficit ΔU changes with $\mathcal{R} - \partial\hat{p}/\partial\hat{x}$, $\mathcal{R}$ and $\int_{-\infty}^{\hat{x}} \mathcal{R} d\xi$ for the simulated baseline case $C_t = 0.6259$, $B = 0.1\%$ and $Ti = 10\%$. The velocity deficit increases approaching the turbine as $\mathcal{R} - \partial\hat{p}/\partial\hat{x}$ is negative, i.e. the pressure gradient is more dominant. $\mathcal{R}$ is zero at the early stage of the induction zone upstream of the disc because the velocity profile still has a flat top. Once the wake becomes more Gaussian-like, $\mathcal{R}$ increases and partially cancels out the effect of the pressure gradient. When $\mathcal{R} - \partial\hat{p}/\partial\hat{x}$ is equal to zero, the centreline velocity deficit reaches its maximum point, after which the velocity begins to recover. For a relatively short distance downstream, the wake recovers at an accelerating rate as $\mathcal{R} - \partial\hat{p}/\partial\hat{x}$ is still increasing. After $\mathcal{R} - \partial\hat{p}/\partial\hat{x}$ reaches its maximum, the wake recovers at a decelerating rate. Since the existing far-wake models predict such a decelerating recovery rate in the far wake, the beginning of the far-wake model should be at the point where $\mathcal{R} - \partial\hat{p}/\partial\hat{x}$ is at its maximum. We find this point approximately as the point where

$$\mathcal{R} = \int_{-\infty}^{\hat{x}} \mathcal{R} d\xi \tag{20}$$

is satisfied. Fei et al. (2025) used the same condition for a single turbine with a Gaussian wake profile placed in an infinitely large domain to predict the start of the far wake.

Equation (20) gives a good approximation of the starting point of the far wake, where we usually observe large $\mathcal{R}$ and small $\partial\hat{p}/\partial\hat{x}$. As shown by Fig. 4, the intersection point between $\mathcal{R}$ and $\int_{-\infty}^{\hat{x}} \mathcal{R} d\xi$ occurs when $\mathcal{R}$ is large, which is also observed for other flow conditions tested in this study except for $Ti = 1\%$. A large shear stress suggests that the wake profile is Gaussian or at least close to Gaussian, and the velocity deficit also needs to be large to sustain the large shear stress, implying that the wake is at an early stage. Also, this point usually occurs downstream of the maximum $\mathcal{R}$ location except for low turbulence

https://doi.org/10.5194/wes-2026-76
Preprint. Discussion started: 13 May 2026

eawe european academy of wind energy
Open Access WIND ENERGY SCIENCE DISCUSSIONS

conditions, such as $Ti = 1\%$ in this study. $\mathcal{R}$ decreases due to decreasing velocity deficit, which means the pressure gradient cannot sustain further reduction in velocity and should be relatively small at that point, so that the pressure can be assumed to have equalised in the streamwise direction. The pressure in the bypass is also assumed to be equal to the pressure in the wake.

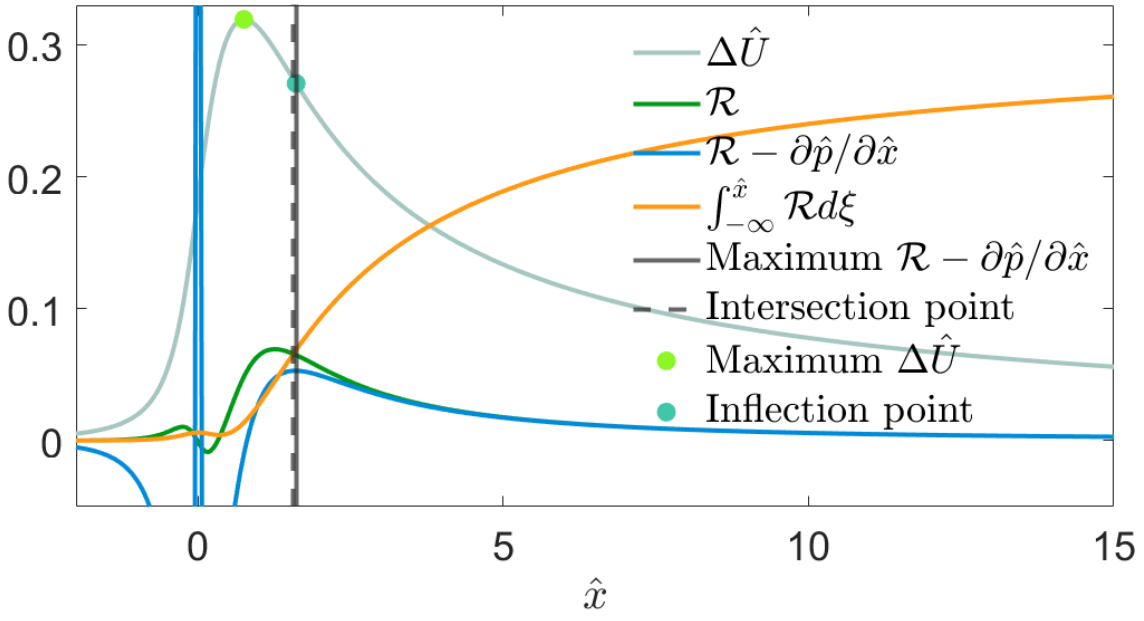

Figure 4. The centreline ΔU, $\mathcal{R}$, $\mathcal{R} - \partial\hat{p}/\partial\hat{x}$, $\int_{-\infty}^{\hat{x}} \mathcal{R}d\xi$, the streamwise location of maximum $\mathcal{R} - \partial\hat{p}/\partial\hat{x}$ and the intersection point between $\int_{-\infty}^{\hat{x}} \mathcal{R}d\hat{x}$ and $\mathcal{R}$ for the baseline case.

The position of the maximum $\mathcal{R} - \partial\hat{p}/\partial\hat{x}$ and the intersection point between $\mathcal{R}$ and $\int_{-\infty}^{\hat{x}} \mathcal{R}d\xi$ are marked by vertical solid and dashed lines respectively in Fig. 4. For most of the flow conditions examined in this study, the streamwise distance between these two points is less than or equal to $0.09D$ except for the case of $C_t = 0.36$ and the case of $Ti = 1\%$ that we simulated, where the distance differences are $0.18D$ and $1.53D$, respectively. The two positions are less close for low inflow turbulence intensities, because $\mathcal{R} = \int_{-\infty}^{\hat{x}} \mathcal{R}d\xi$ occurs before the wake profile becomes fully Gaussian, and $\mathcal{R}$ continues to increase for a while before $\mathcal{R} - \partial\hat{p}/\partial\hat{x}$ reaches its maximum value.

3.3 Streamwise position of the start of far wake

With a clear definition of Stage 3 and a way to model $\int_{-\infty}^{\hat{x}_3} \mathcal{R}d\hat{x}$, we can calculate the velocity profile using Eq. (17), (18), (19). Now, we also need to find the position of Stage 3. We take the derivative of both sides of Eq. (20) with respect to $\hat{x}_3$, which gives

$$\left(\frac{\partial\mathcal{R}}{\partial\hat{x}}\right)_3 = \mathcal{R}_3 \tag{21}$$

https://doi.org/10.5194/wes-2026-76
Preprint. Discussion started: 13 May 2026

eawe european academy of wind energy
Open Access WIND ENERGY SCIENCE DISCUSSIONS

Here, the suffix 3 is added because for a given turbine case, this relationship holds only at Stage 3. Then, using this relationship and the theorem for implicit function (Krantz and Parks, 2002), we can find how the position of Stage 3 varies with eddy viscosity. According to the theorem for implicit function,

$$\frac{\partial \hat{x}_3}{\partial \hat{\nu}_{t_3}} = -\frac{\partial \mathcal{R}_3/\partial \hat{\nu}_{t_3}}{\partial \mathcal{R}_3/\partial \hat{x}_3}. \tag{22}$$

By inserting Eq. (22) into Eq. (21) for $\partial \mathcal{R}_3/\partial \hat{x}_3$, there is

$$\frac{\partial \hat{x}_3}{\partial \mathcal{R}_3} = -\frac{1}{\mathcal{R}_3}. \tag{23}$$

Note that Eq. (21) and (23) have different physical meanings. Equation (21) describes the position of Stage 3, where this relationship holds for given flow conditions. Equation (23) describes how the point where Eq. (21) holds changes with different inflow turbulence intensities, i.e., the flow conditions are not fixed. Equation (23) can be integrated to give

$$\hat{x}_3 = -\ln(\mathcal{R}_3) + const. \tag{24}$$

Then we use a boundary condition (in terms of the possible range of ν_{t_3}) to find the constant of integration. When $\hat{\nu}_{t_3}$ tends to zero, the flow is inviscid, and the wake cannot recover, so $\hat{x}_3$ should be at infinity. This condition is naturally satisfied by the equation. The other extreme case occurs when $\hat{\nu}_{t_3}$ is sufficiently large so that when the turbine causes any velocity deficit, the mixing effect recovers it instantly. In that case, there will be no wake, which means all five stages coincide together at the disc, hence $\hat{x}_3 = 0$. The corresponding $\mathcal{R}_3$ is equal to $\int_{-\infty}^{\infty} \mathcal{R} d\hat{x}$, which can be found by Eq. (15) at $\hat{x} = \infty$. When $\hat{x} = \infty$, $\alpha = 1$, so that

$$\hat{p}_2^+ - \hat{p}_2^- = \hat{p}_0 - \hat{p}_5 + \int_{-\infty}^{\infty} \mathcal{R} d\hat{x}, \tag{25}$$

and

$$\int_{-\infty}^{\infty} \mathcal{R} d\hat{x} = \frac{T}{\rho U_0^2 A_D} - \frac{T}{\rho U_0^2 A_c} = \frac{(1-B)C_t}{2}. \tag{26}$$

Hence, we can find the relationship between the position of Stage 3 (start of the far wake) and the turbulent eddy viscosity as

$$\hat{x}_3 = -\ln(\mathcal{R}_3) + \ln\left(\frac{(1-B)C_t}{2}\right), \tag{27}$$

which can be rearranged as

$$\mathcal{R}_3 = 2\hat{\nu}_{t_3}\frac{C_3}{(\sigma_3/D)^2} = \frac{(1-B)C_t}{2}e^{-\hat{x}_3}. \tag{28}$$

https://doi.org/10.5194/wes-2026-76
Preprint. Discussion started: 13 May 2026

eawe european academy of wind energy
Open Access WIND ENERGY SCIENCE DISCUSSIONS

3.4 Far-wake model

After finding the velocity profile at Stage 3 and its streamwise position, we can now calculate the rest of the flow field using a marching method, which considers a series of consecutive control volumes in the centreline streamtube. The reason we use such an approach is that we can consider the momentum and mass conservation of the entire cross-sectional domain, so that the blockage effect can be considered. The inlet of the first control volume is located at Stage 3, where the values of α_3, β_3 and σ_3 are known, and we march the solution to the outlet of the control volume which will be used as the inlet for the next control volume. The process repeats until the entire far wake flow is solved.

We start with Eq. (10) at the wake centreline, drop the pressure gradient term since it is negligible in the far-wake region, and rearrange the equation as

$$\frac{\partial \alpha}{\partial \hat{x}} = \frac{\mathcal{R}}{\alpha}. \tag{29}$$

Then we integrate this equation from the inlet to the outlet of the control volume located at the wake centre. Using a first-order Taylor expansion, there is

$$\alpha_{i+1} = \alpha_i + \frac{\mathcal{R}}{\alpha_i}\Delta\hat{x} \tag{30}$$

where the suffix i denotes the position at the inlet of the control volume and $i+1$ denotes the position at the outlet of the control volume.

Then, we also need to calculate how β and σ vary in this process. We calculate β_{i+1} and σ_{i+1} by solving mass conservation and momentum conservation with α_{i+1} simultaneously. The calculated α_{i+1}, β_{i+1} and σ_{i+1} will be used as inlet conditions for the next control volume, and the process repeats until the entire far wake flow is solved.

3.5 Eddy viscosity model

We also require the centreline eddy viscosity as an input for this model. Some of the commonly used wake-induced turbulence models are listed by Sørensen et al. (2008). For this work, the eddy viscosity model from Gunn (2019) with a modification is used as an example. The original model is formulated as follows.

$$\nu_t = F(K_l + K_a) \tag{31}$$

where

$$K_l = k_1 b U_0 C, \tag{32}$$

k_1 is an empirical constant equal to 0.015, b is the wake width equal to $\sqrt{7.12}\sigma$, F is a filter function which is

$$F = 0.65 + \left(\frac{\hat{x} - 4.5}{23.32}\right)^{1/3} \tag{33}$$

https://doi.org/10.5194/wes-2026-76
Preprint. Discussion started: 13 May 2026

eawe european academy of wind energy
Open Access WIND ENERGY SCIENCE DISCUSSIONS

for $\hat{x} < 5.5$ and $F = 1$ for $\hat{x} \geq 5.5$, and

$$K_a = k_a I_0 U_0 l_0 \tag{34}$$

where $k_a = 0.5$ is a dimensionless constant recommended by Gunn (2019), I_0 is the ambient turbulence intensity, and l_0 is the mixing length. In this study, we take $I_0 = Ti$ and $l_0 = l$, where Ti and l are the turbulence intensity and the mixing length at the inlet of the computational domain. Since the empirical constant of the above eddy viscosity model is not found by RANS simulations with $k - \epsilon$ model as used in this study, the ambient component FK_a does not match the ambient eddy viscosity in our RANS simulations, where we added source terms for k and ϵ to maintain the ambient turbulence level (see Section 2). For a fair comparison with the RANS simulation used in this study, we change F to a constant value of 1.3416 to match the ambient eddy viscosity. The rest of the model is unchanged from Gunn (2019).

3.6 Modifications to the momentum deficit conservation

Due to the discrepancies between the wake profile from the simulation and the Gaussian profile, the wake characteristic width σ calculated from the unmodified model does not match the simulation very well. This inaccuracy directly affects the accuracy of $\mathcal{R}$ and results in discrepancies in the prediction of wake recovery. Since we are interested in the velocity in the wake region and the wake width, we propose some modifications to Eq. (19) to achieve a more accurate solution of the wake profile close to the wake centre and better evaluation of $\mathcal{R}$.

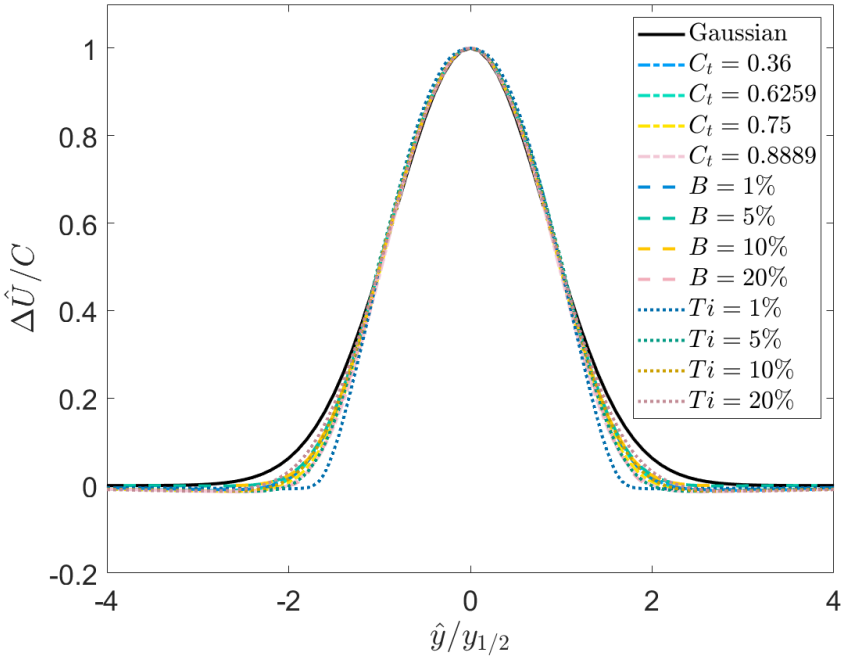

Figure 5. The comparison between RANS far wake profiles for different flow conditions and the Gaussian profile.

https://doi.org/10.5194/wes-2026-76
Preprint. Discussion started: 13 May 2026

eawe european academy of wind energy
Open Access WIND ENERGY SCIENCE DISCUSSIONS

Before deciding on the modification, we first analyse the cause of this profile discrepancy. The Gaussian wake profile is a solution to the simplified momentum equation (Pope, 2000). One of the assumptions is that the eddy viscosity is constant in the spanwise direction. However, for a more realistic wake flow, the eddy viscosity is higher in the wake region due to the wake-induced turbulence. The Gaussian profile thus does not agree with the simulation wake profile well around the wake edge. We plot the velocity deficit normalised by the centreline velocity deficit against $\hat{y}$ normalised by the half-width of the wake, $y_{1/2}$, which is defined as the width where the velocity deficit is half of the centreline velocity deficit, in Fig. 5 to show this discrepancy. The simulation results suggest that a matching Gaussian profile overestimates the momentum deficit flux. The modified model should account for this overestimation.

The original expression for $T-(p_0-p)A_c$ in Eq. (19) is $T-\frac{1}{2}\rho(\beta^2-1)U_0^2A_c$, which is derived from the Bernoulli equation. A simple modification would be to use $T-\frac{1}{2}\rho(\beta-1)(\beta+2\alpha-1)U_0^2A_c$ instead, where the pressure drop term has the same form as p_0-p_5 derived by Garrett and Cummins (2007), and approximates the pressure difference between the blocked case and the unblocked case. However, this modification works less well for high thrust coefficients. Since for some flow conditions, $\frac{1}{2}(\beta^2-1)$ tends to underestimate $\mathcal{R}$, and $\frac{1}{2}(\beta-1)(\beta+2\alpha-1)$ tends to overestimate $\mathcal{R}$, we take the average of the two for the model to be robust. The final modified term is $T-\frac{1}{2}\rho(\beta-1)(\beta+\alpha)U_0^2A_c$. Currently, there is no strict explanation for the validity of this expression.

3.7 Implementation

The following steps describe how the proposed model has been implemented in our MATLAB code:

1. Specify the input parameters: Ti, l, C_t, U_0, A_D, L_y and L_z, where L_z and L_y are the half lengths of the domain size in the vertical and horizontal direction, respectively.

2. Solve the following three equations (that are obtained by inserting Eq. (6) into Eq. (17), (18) and (19)) to calculate the initial far-wake profile at Stage 3, i.e. α_3, β_3 and σ_3.

$$C_t = \beta^2-\alpha^2+4\hat{\nu}_{t_3}\frac{C}{(\sigma/D)^2}, \tag{35}$$

$$4\beta L_yL_z-2\pi C\sigma^2\,\mathrm{erf}(\frac{L_y}{\sqrt{2}\sigma})\,\mathrm{erf}(\frac{L_z}{\sqrt{2}\sigma})=A_c, \tag{36}$$

and

$$\frac{2\beta(1-\beta)}{B}+C(2\beta-1)\frac{4\pi\sigma^2}{A_D}\,\mathrm{erf}(\frac{L_z}{\sqrt{2}\sigma})\,\mathrm{erf}(\frac{L_y}{\sqrt{2}\sigma})-C^2\frac{2\pi\sigma^2}{A_D}\,\mathrm{erf}(\frac{L_z}{\sigma})\,\mathrm{erf}(\frac{L_y}{\sigma}) \tag{37}$$
$$=C_t-\frac{(\beta-1)(\beta+\alpha)}{B},$$

where $\hat{\nu}_{t_3}$ is expressed in terms of C and σ using the model described in Section 3.5. The MATLAB function $vpasolve$ is used to solve the equation system.

3. With known α_3, β_3, σ_3, D, C_t, L_y, L_z and U_0, use Eq. (27) to calculate the initial far-wake position $\hat{x}_3$, where $\mathcal{R}_3$ is $\hat{\nu}_{t_3}\frac{C_3}{(\sigma_3/D)^2}$, and is found by inserting Eq. (6) into Eq. (12).

https://doi.org/10.5194/wes-2026-76
Preprint. Discussion started: 13 May 2026

eawe european academy of wind energy
Open Access WIND ENERGY SCIENCE DISCUSSIONS

4. With known α_i, β_i, σ_i, $\hat{x}_i$, and given a marching step size $\Delta\hat{x}$, calculate α_{i+1} by inserting Eq. (6) into Eq. (30)

$$\alpha_{i+1} = \alpha_i + 2\frac{\hat{\nu}_{t_i}}{\alpha_i}\frac{C_i}{(\sigma_i/D)^2}\Delta\hat{x}, \tag{38}$$

where $\hat{\nu}_{t_i}$ is calculated by C_i and σ_i using the model described by Section 3.5. Update the streamwise position as $\hat{x}_{i+1} = \hat{x}_i + \Delta\hat{x}$.

5. Use Eq. (36) and (37) to solve for β_{i+1} and σ_{i+1}. The two equations are solved simultaneously with the MATLAB function $fsolve$.

6. With α_{i+1}, β_{i+1}, σ_{i+1} and $\hat{x}_{i+1}$, repeat Steps 4 to 5 until the entire far wake flow is solved.

4 Results and discussion

4.1 Near wake prediction

We first verify the near-wake model by examining how well Eq. (28) predicts the intersection point between $\mathcal{R}$ and $\int_{-\infty}^{\hat{x}} \mathcal{R}d\xi$. Figure 6 presents the analytical solution to the intersection point for a range of inflow turbulence intensities. Equation (28) predicts only one curve for varying inflow turbulence intensities. For the inflow turbulence intensities simulated, the intersection points between $\mathcal{R}$ and $\int_{-\infty}^{\hat{x}} \mathcal{R}d\xi$ collapse onto the analytical solution well. As the turbulence intensity increases, the shear stresses also increase, and the wake transitions to the far wake faster, so that the intersection point gets closer to the disc. This trend is well captured by the model.

Results for different thrust coefficients are presented in Fig. 7. Each C_t has its own analytical curve, and the intersection points between $\mathcal{R}$ and $\int_{-\infty}^{\hat{x}} \mathcal{R}d\xi$ are well predicted by each analytical solution. As the thrust coefficient increases, the intersection point gets closer to the disc. Such behaviour is expected since a large thrust coefficient generates larger shear stresses, and the near wake transitions to the far wake faster.

For varying blockage ratios, the intersection points between $\mathcal{R}$ and $\int_{-\infty}^{x} \mathcal{R}d\xi$ do not change much up to $B = 20\%$ as shown in Fig. 8. As the blockage ratio increases, the intersection position moves downstream slightly. According to Eq. (28), increasing B is analogous to decreasing C_t, which increases the near-wake length. However, since $\mathcal{R}_3$ does not change much with increasing B for the cases in this study, the intersection points from the simulation collapse less well to the analytical curve compared to the cases for varying Ti and C_t. In Sections 4.2 and 4.3, we will show that the accuracy in the far wake region is not greatly affected by this inaccuracy at the beginning of the far wake.

https://doi.org/10.5194/wes-2026-76
Preprint. Discussion started: 13 May 2026

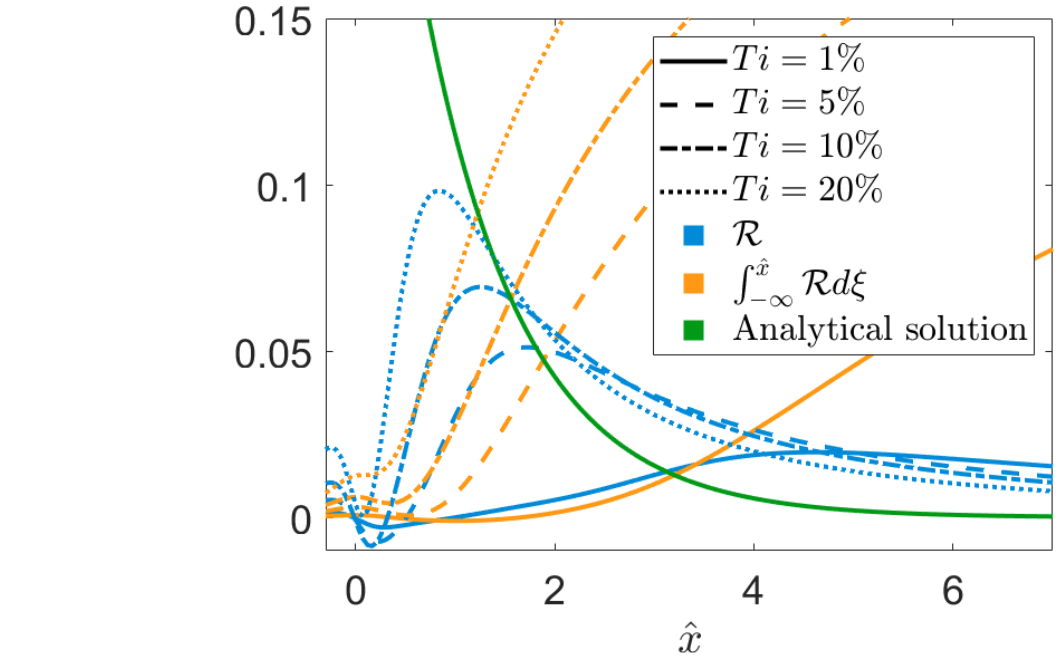

Figure 6. Analytical prediction of the intersection points between $\mathcal{R}$ and $\int_{-\infty}^{\hat{x}} \mathcal{R} d\xi$ for different inflow turbulence intensities with $B = 0.1\%$ and $C_t = 0.6259$.

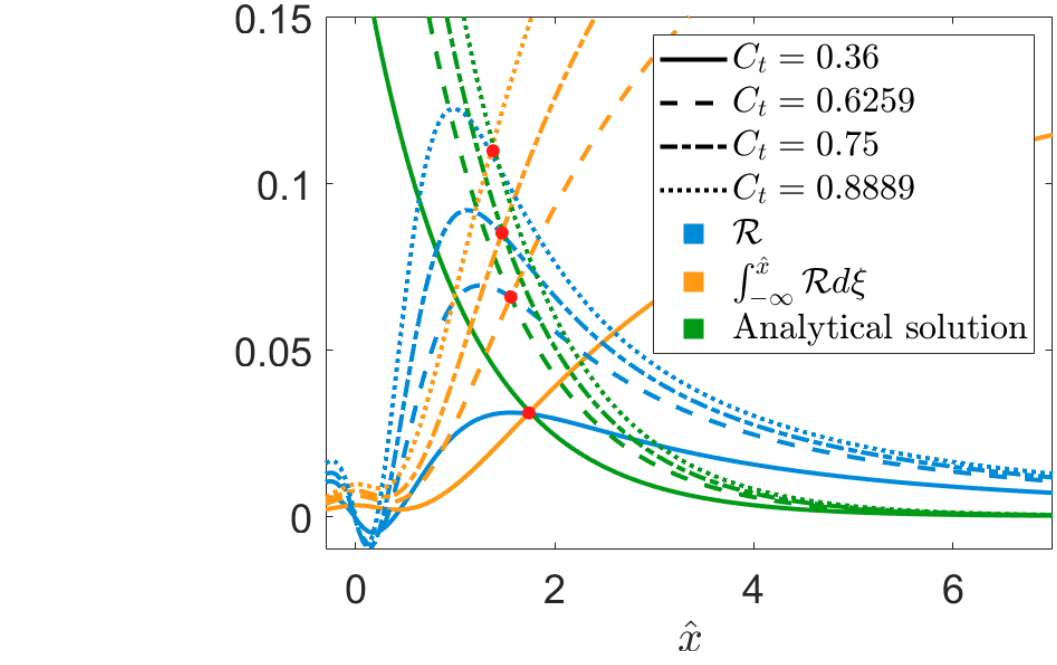

Figure 7. Analytical prediction of the intersection points between $\mathcal{R}$ and $\int_{-\infty}^{\hat{x}} \mathcal{R} d\xi$ for different thrust coefficients with $Ti = 10\%$ and $B = 0.1\%$. The intersection points are marked by red dots for clarity.

https://doi.org/10.5194/wes-2026-76
Preprint. Discussion started: 13 May 2026

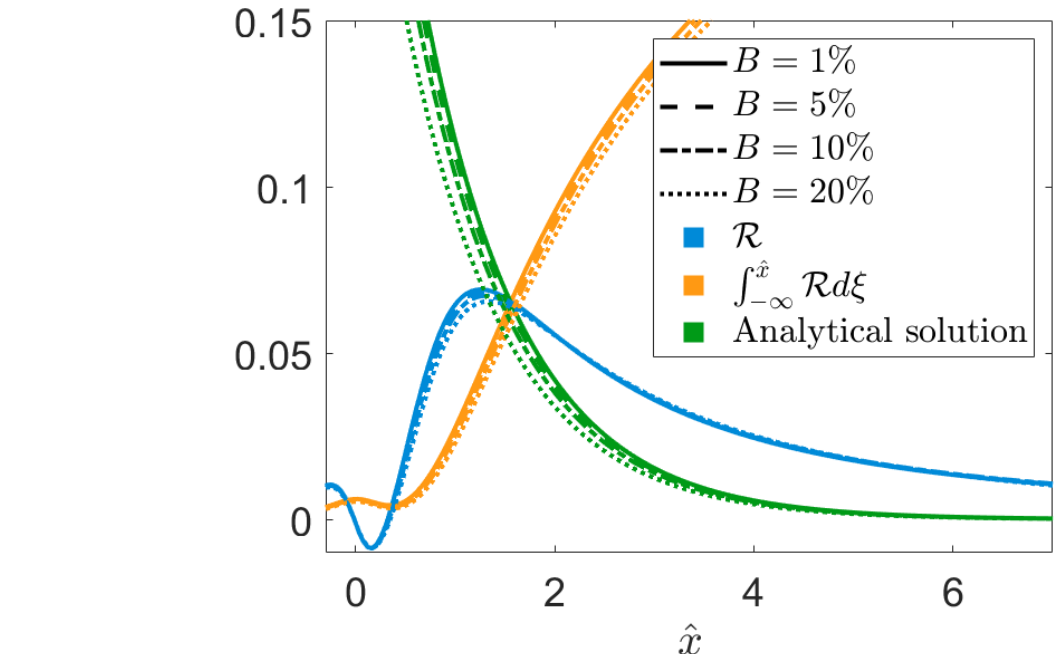

Figure 8. Analytical prediction of the intersection points between $\mathcal{R}$ and $\int_{-\infty}^{\hat{x}} \mathcal{R} d\xi$ for different blockage ratios with $Ti = 10\%$ and $C_t = 0.6259$.

4.2 Centreline velocity prediction

Here we use the proposed wake model with two different options for the eddy viscosity: one obtained from the RANS simulations $\nu_{t_{sim}}$, and the other from the model described in Section 3.5, $\nu_{t_{model}}$. We first compare the wake centreline velocity against the results of the RANS simulations and the Bastankhah and Porté-Agel (2014) model, which is referred to as the BP model in the following. In this study, the BP model adopts the analytical solution $\sigma_0 = 0.25\sqrt{0.5(1+\sqrt{1-C_t})/(\sqrt{1-C_t})}$ (Bastankhah and Porté-Agel, 2014) as the initial wake width, and $d\sigma/dx = 0.003678 + 0.3837Ti$ as the wake expansion rate, which is used by Ali et al. (2024). To quantitatively evaluate the model performance, Table 3 shows the root mean square error e_{rms} and the maximum error e_{max} of each model for each thrust coefficient, which are defined as

$$e_{rms} = \frac{1}{n}\sum_{i=1}^{n}\sqrt{\frac{|\,\hat{U}_{model} - \hat{U}_{sim}\,|^2}{|\,\hat{U}_{sim}\,|^2}} \times 100\% \tag{39}$$

and

$$e_{max} = \frac{|\,\hat{U}_{model} - \hat{U}_{sim}\,|}{|\,\hat{U}_{sim}\,|} \times 100\%, \tag{40}$$

where $\hat{U}_{model}$ is the model predicted centreline velocity, $\hat{U}_{sim}$ is the simulation centreline velocity, i denotes the data point being calculated, and n is the total number of data points at which we model the wake velocity along the streamwise direction. n is between 630 and 640, depending on the specific case.

https://doi.org/10.5194/wes-2026-76
Preprint. Discussion started: 13 May 2026

eawe european academy of wind energy
Open Access WIND ENERGY SCIENCE DISCUSSIONS

Figure 9 shows the results for a range of thrust coefficients. For all the thrust coefficients examined, the proposed model with both eddy viscosity inputs provides good accuracy. As the thrust coefficient increases, the velocity at the start of the far wake decreases. This trend is captured well by the proposed model. While the BP model provides good predictions for $C_t = 0.36, 0.6259$ and 0.75, it significantly overpredicts the velocity at the beginning of the far wake for $C_t = 0.8889$. This overprediction is partly due to neglecting the wake-induced turbulence intensity.

For all the thrust coefficients examined, the e_{rms} of the proposed model with either eddy viscosity sub-model is less than 1.5% and always smaller than that of the BP model. This suggests that the proposed model is applicable to various thrust coefficients and is generally robust. The e_{max} values of the proposed model for either ν_t input do not exceed 1.5% for $C_t = 0.36$ and $C_t = 0.6259$. For higher thrust coefficients, e_{max} increases and mainly appears close to the start of the far wake. Thus, although the near-wake model can capture how the start of the far wake varies (Stage 3), the accuracy still decreases a little with increasing C_t. Still, the largest e_{max} of the proposed model is 8.17%, which is considerably smaller than the largest e_{max} of the BP model, which is 19.79%. The large error in the BP model mainly comes from the poor estimation of the wake width at the start of the far wake.

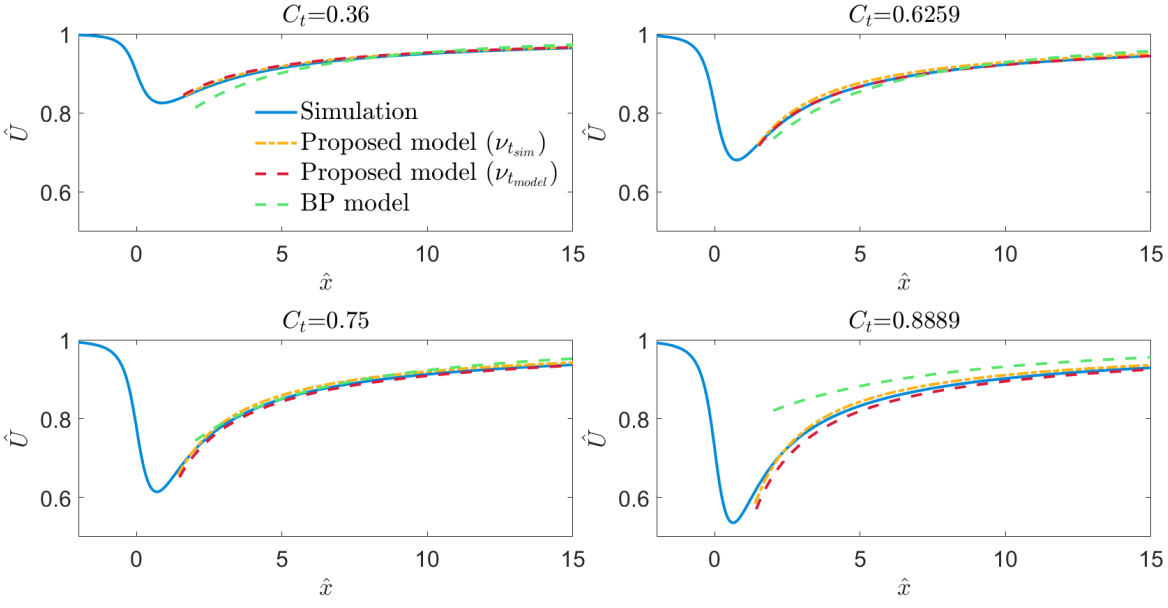

Figure 9. Comparison of the centreline velocity predicted by the RANS simulations and wake models for a range of thrust coefficients.

Figure 10 compares the centreline velocity predicted by the wake models against the RANS simulation results over a range of inflow turbulence conditions. All models are challenged when predicting the case of low inflow turbulence intensity of $Ti = 1\%$. For the proposed model, the inaccuracy is inherited from the start of the far wake and attributed to the super-Gaussian, rather than Gaussian, wake profile at Stage 3. Thus, the predicted $\mathcal{R}_3$ does not give an accurate centreline velocity nor an accurate streamwise position. This error is even more apparent for the case with modelled eddy viscosity input, since ν_t

https://doi.org/10.5194/wes-2026-76
Preprint. Discussion started: 13 May 2026

eawe european academy of wind energy
Open Access WIND ENERGY SCIENCE DISCUSSIONS

Table 3. Root mean square error e_{rms} and the maximum error e_{max} of each model for different thrust coefficients (with $Ti = 10\%$ and $B = 0.1\%$).

C_t	0.36		0.6259		0.75		0.8889	
	e_{rms}	e_{max}	e_{rms}	e_{max}	e_{rms}	e_{max}	e_{rms}	e_{max}
Proposed model ($\nu_{t_{sim}}$)	0.27%	0.64%	0.62%	1.22%	0.67%	1.84%	0.87%	5.10%
Proposed model ($\nu_{t_{model}}$)	0.35%	0.99%	0.08%	0.84%	0.55%	3.41%	1.34%	8.17%
BP model	1.26%	4.66%	1.49%	3.03%	1.58%	3.24%	4.69%	19.79%

is also overestimated. For the BP model, the difference with the RANS simulation is greater in the far wake, partly due to the difference in expansion rate in the near and far wake.

For higher turbulence intensities, the proposed model with either eddy viscosity input produces accurate results. The BP model is less accurate than the proposed model for $Ti = 5\%$, but comparatively accurate for $Ti = 10\%$ and $Ti = 20\%$. The e_{rms} of the proposed model for either eddy viscosity input does not exceed 2%, and the maximum e_{max} is 2.76%. For $Ti = 5\%$, 10% and 20%, the proposed model has smaller e_{rms} than the BP model. For $Ti = 5\%$ and $Ti = 10\%$, the e_{max} of the proposed model is also smaller than the BP model.

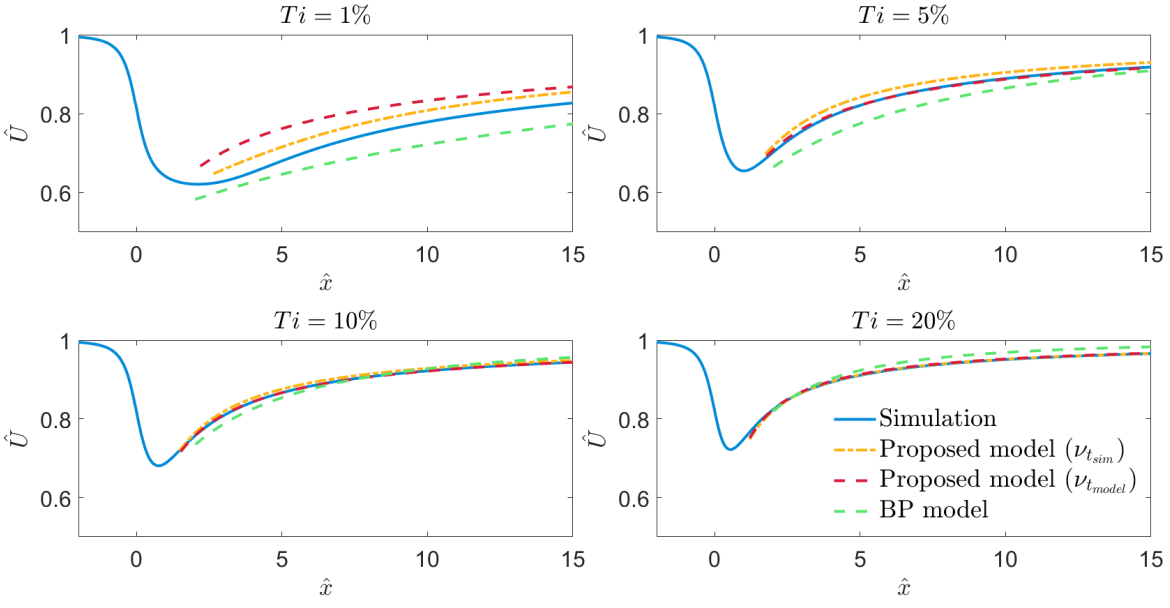

Figure 10. Comparison of the centreline velocity predicted by the RANS simulations and wake models for a range of inflow turbulence intensities.

https://doi.org/10.5194/wes-2026-76
Preprint. Discussion started: 13 May 2026

eawe european academy of wind energy
Open Access WIND ENERGY SCIENCE DISCUSSIONS

Table 4. Root mean square error e_{rms} and the maximum error e_{max} of each model for different inflow turbulence intensities (with $C_t = 0.6259$ and $B = 0.1\%$).

Ti	1%		5%		10%		20%	
	e_{rms}	e_{max}	e_{rms}	e_{max}	e_{rms}	e_{max}	e_{rms}	e_{max}
Proposed model ($\nu_{t_{sim}}$)	3.61%	5.63%	1.57%	2.76%	0.62%	1.22%	0.23%	2.38%
Proposed model ($\nu_{t_{model}}$)	6.59%	13.04%	0.26%	0.96%	0.08%	0.84%	0.20%	1.97%
BP model	5.50%	7.35%	2.77%	6.16%	1.49%	3.03%	1.56%	1.89%

Figure 11 shows the same comparison for different blockage ratios. As the blockage ratio increases, the wake velocity increases, and this trend is captured by the proposed model. For all the blockage ratios examined, the proposed model with either eddy viscosity input provides accurate solutions. The accuracy at the start of the far wake reduces slightly as the blockage ratio increases. This is because the near-wake model does not fully capture the relationship between $\mathcal{R}_3$ and B, as described in Section 4.1. Figure 11 also shows that the inaccuracy gradually reduces as the wake develops further into the far-wake region. The BP model gives the same solution for each case, because the model does not consider the blockage effect. Thus, as the blockage effect increases, the BP model underestimates the centreline velocity. The proposed model with either eddy viscosity inputs has lower e_{rms} and e_{max} values than the BP model for all the blockage ratios examined, as shown in Table 5.

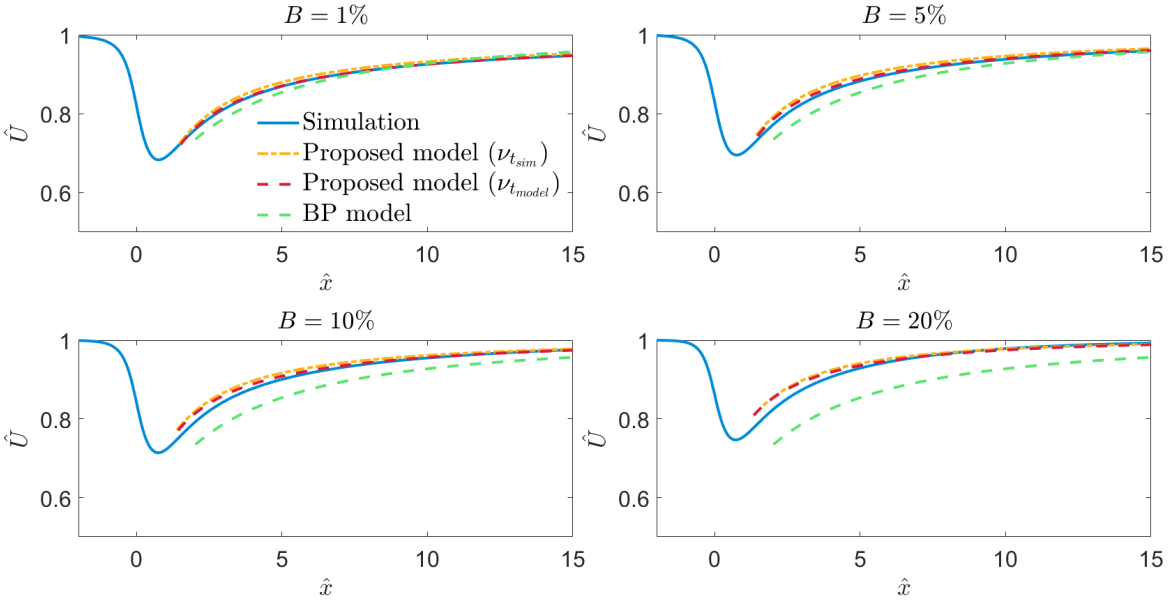

Figure 11. Comparison of the centreline velocity predicted by the RANS simulations and wake models for a range of blockage ratios.

https://doi.org/10.5194/wes-2026-76
Preprint. Discussion started: 13 May 2026

eawe european academy of wind energy
Open Access WIND ENERGY SCIENCE DISCUSSIONS

Table 5. Root mean square error e_{rms} and the maximum error e_{max} of each model for different blockage ratios (with $Ti = 10\%$ and $C_t = 0.6259$).

B	1%		5%		10%		20%	
	e_{rms}	e_{max}	e_{rms}	e_{max}	e_{rms}	e_{max}	e_{rms}	e_{max}
Proposed model ($\nu_{t_{sim}}$)	0.71%	1.49%	0.98%	2.55%	1.12%	3.53%	1.06%	4.10%
Proposed model ($\nu_{t_{model}}$)	0.14%	0.52%	0.47%	1.75%	0.75%	2.88%	0.94%	4.09%
BP model	1.36%	3.32%	1.66%	4.93%	3.03%	7.28%	4.90%	10.88%

4.3 Velocity along the spanwise direction

Next, we examine the velocity profile along the spanwise direction at Stage 3 and $5D$ downstream of the turbine for different flow conditions. Figure 12 compares the model predictions against the simulation results and the BP model predictions over a range of turbulence conditions. As the turbulence intensity increases, the wake recovers faster as expected. At Stage 3, the proposed model with both eddy viscosity inputs predicts both the wake centreline velocity and the wake width well from $Ti = 5\%$ to $Ti = 20\%$. The BP model also yields accurate results, but the centreline velocity is slightly underestimated. At $\hat{x} = 5$, the proposed model predicts an accurate wake profile from $Ti = 5\%$ to $Ti = 20\%$. The BP model underestimates the wake velocity around the centre at $Ti = 5\%$, but predicts accurate wake profiles for $Ti = 10\%$ and $Ti = 20\%$. Note that the BP model underestimates the centreline velocity at both Stage 3 and $\hat{x} = 5$, so the inaccuracy primarily comes from the initial wake width rather than the wake expansion rate. Thus, an accurate and general near-wake model is important for far wake prediction.

https://doi.org/10.5194/wes-2026-76
Preprint. Discussion started: 13 May 2026

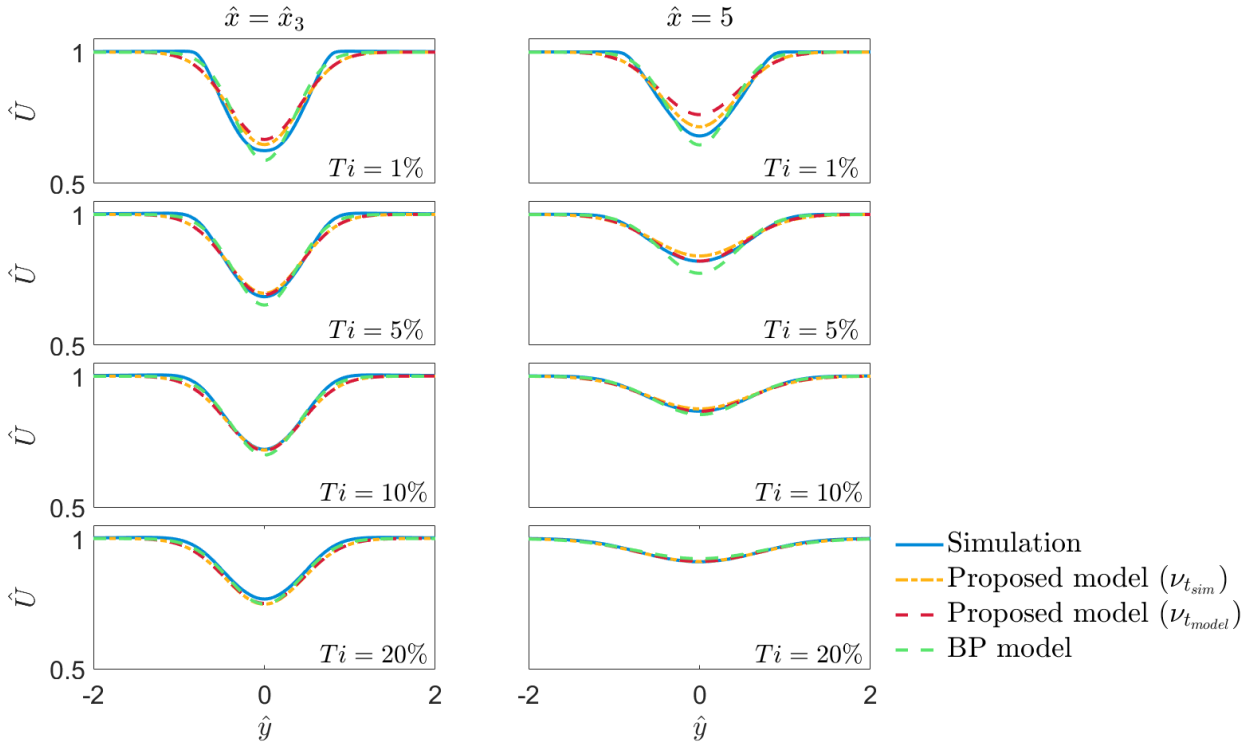

Figure 12. Comparison of velocity profiles at Stage 3 and $\hat{x} = 5$ for a range of inflow turbulence conditions.

For $Ti = 1\%$, both wake models perform less well compared to the higher Ti cases. For the proposed model, the accuracy reduces because the wake profile is not fully Gaussian at Stage 3, as shown in Fig. 12. The model assumes a Gaussian wake profile, which leads to an overestimated $\int_{-\infty}^{\hat{x}_3} \mathcal{R} d\hat{x}$, so that the wake centreline velocity is overestimated. This is also why the results with the model eddy viscosity more significantly overestimate the centreline velocity, because the eddy viscosity is also overestimated. The effect of the overestimation accumulates and is reflected in the wake profile at $5D$. For the BP model, the performance reduces because the wake around Stage 3 expands non-linearly.

Figure 13 shows the velocity profile along the spanwise direction for Stage 3 and $\hat{x} = 5$ for different blockage ratios. As the blockage ratio increases, the bypass velocity increases, which is captured by the proposed model but not considered by the BP model. This is why the BP model gradually underestimates the wake velocity as the blockage ratio increases. Both the wake width and the velocity deficit do not vary much, which explains why the streamwise variation of $\mathcal{R}$ does not vary much, as shown in Fig. 8. The proposed model overestimates the centreline velocity as the blockage ratio increases at Stage 3, because the near-wake model does not capture the variation of the intersection point between $\mathcal{R}$ and $\int_{\infty}^{\hat{x}} \mathcal{R} d\xi$ with blockage ratio. As the wake evolves downstream, this overestimation reduces, and the predictions for both velocity magnitude and wake width are accurate.

https://doi.org/10.5194/wes-2026-76
Preprint. Discussion started: 13 May 2026

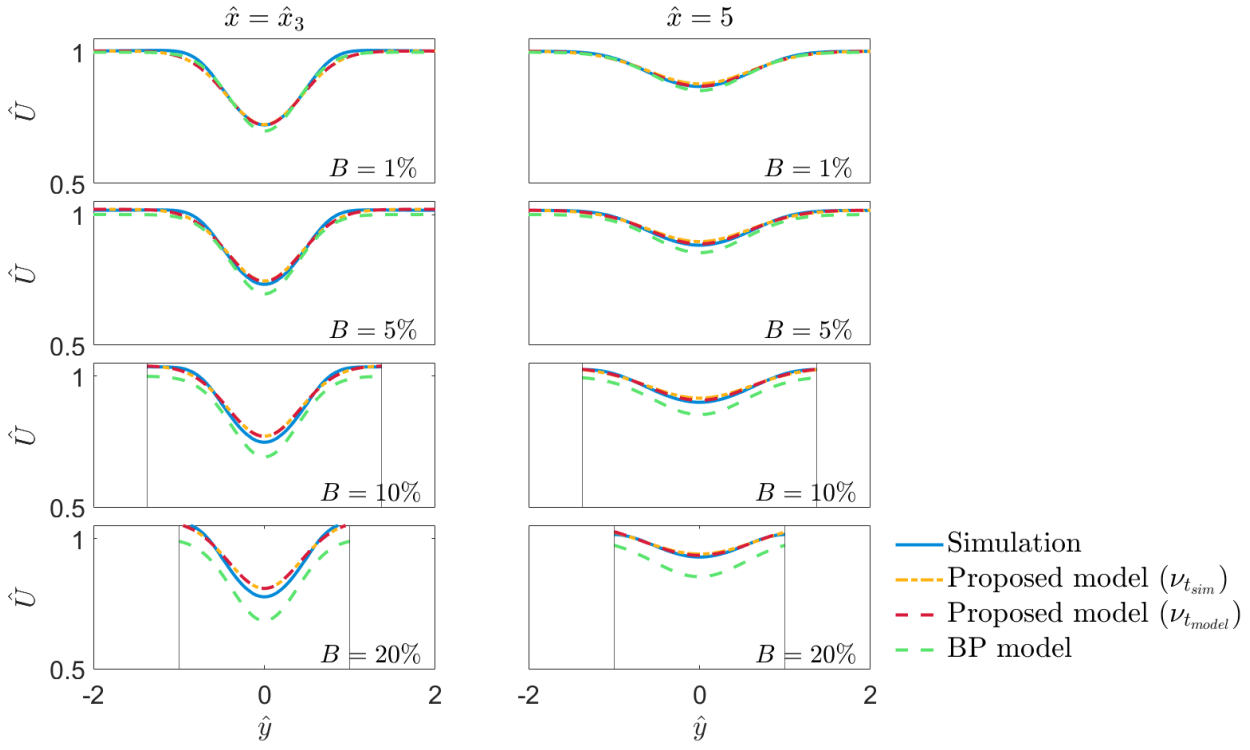

Figure 13. Comparison of velocity profiles at Stage 3 and $\hat{x} = 5$ for a range of blockage ratios, where the vertical black lines denote the domain boundary for $B = 10\%$ and 20%.

The same comparisons between the simulation and different model predictions for varying thrust coefficients are presented in Fig. 14. The proposed model with both eddy viscosity inputs predicts accurate velocity profiles for all the thrust coefficients examined at both Stage 3 and $\hat{x} = 5$. The BP model slightly underestimates the centreline velocity at $C_t = 0.36$. As the thrust coefficient increases, the BP model gradually overestimates the centreline velocity, especially for $C_t = 0.8889$. The BP model is less adaptive to varying thrust coefficients, partly because the model does not consider the wake-induced turbulence, and the wake expansion rate for the BP model used in this study only considers the effect of ambient turbulence intensity. This study, thus, highlights the importance of rotor thrust on the wake expansion rate.

https://doi.org/10.5194/wes-2026-76
Preprint. Discussion started: 13 May 2026

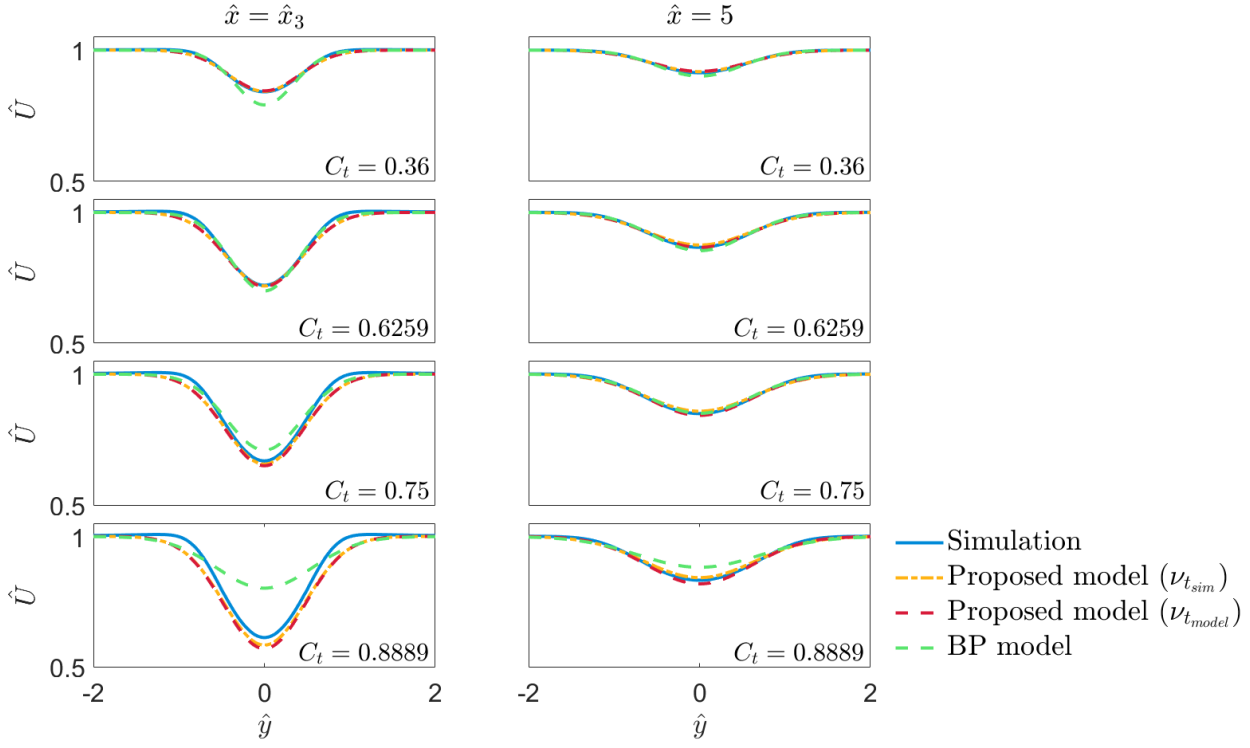

Figure 14. Comparison of velocity profiles at Stage 3 and $\hat{x} = 5$ for a range of thrust coefficients.

5 Conclusions

In this study, we have developed a new analytical method to predict the wake of an actuator disc for a wide range of inflow turbulence intensities, thrust coefficients and blockage ratios. The proposed wake model requires an eddy viscosity model to predict wake recovery. We find the start of the far wake at the position where the divergence of the Reynolds shear stress, $\mathcal{R}$, satisfies the condition $\mathcal{R} = \int_{-\infty}^{\hat{x}} \mathcal{R} d\xi$. This condition occurs around the point where $\mathcal{R} - \frac{\partial \hat{p}}{\partial \hat{x}}$ is maximum. Downstream of this point, the rate of flow speed recovery decreases, which is a characteristic of the far-wake region. The proposed condition provides an analytical solution to the position where this relation holds, and allows us to model the energy transported by turbulent mixing into the wake centreline analytically, so that the corresponding velocity profile can be calculated. We have also proposed a new far-wake model taking into account the local blockage effect by extending the model proposed by Anderson (2009).

For most of the flow conditions examined, the proposed model was found to predict the starting point for the far wake successfully and also predict the variation of the far wake centreline velocity accurately until the wake fully recovers. However, the model performs less well for low turbulence intensities, since the assumption of a Gaussian wake profile is not fully satisfied at the start of the far wake. Through comparison with another analytical wake model and RANS simulation results, we showed

https://doi.org/10.5194/wes-2026-76
Preprint. Discussion started: 13 May 2026

that the near-wake model is important for far-wake prediction, and the thrust coefficient affects the wake expansion rate. We also showed that the blockage effect leads to a non-negligible increase in the wake and bypass flow speeds, and should be considered by the wake model. In future work, it would be interesting to consider a more realistic turbine instead of an actuator disc.

Code and data availability. The model code can be found at https://github.com/Okeraa/Wind-turbine-wake-model-with-blockage.git, with the verification data included.

Author contributions. ZF, TN and CRV jointly developed the theoretical model. ZF carried out the simulations and wrote the manuscript with corrections from TN and CRV.

Competing interests. The authors declare that they have no conflict of interest.

Acknowledgements. This work was partly supported through CRV's UKRI Future Leader's Fellowship MR/V02504X/1.

https://doi.org/10.5194/wes-2026-76
Preprint. Discussion started: 13 May 2026

References

Abramovich, G. N., Girshovich, T., Krasheninnikov, S. I., Sekundov, A., and Smirnova, I.: The theory of turbulent jets, Moscow Izdatel Nauka, 1984.

Ainslie, J. F.: Calculating the flowfield in the wake of wind turbines, Journal of Wind Engineering and Industrial Aerodynamics, 27, 213–224, 1988.

Ali, K., Stallard, T., and Ouro, P.: A diffusion-based wind turbine wake model, Journal of Fluid Mechanics, 1001, A13, 2024.

Anderson, M.: Simplified solution to the eddy-viscosity wake model, Tech. rep., Global Renewable Energy Solution company, 2009.

Bastankhah, M. and Porté-Agel, F.: A new analytical model for wind-turbine wakes, Renewable Energy, 70, 116–123, 2014.

Blondel, F. and Cathelain, M.: An alternative form of the super-Gaussian wind turbine wake model, Wind Energy Science, 5, 1225–1236, 2020.

Fei, Z., Nishino, T., and Vogel, C.: Analytical prediction of the start of a wind turbine far wake considering the balance between pressure and Reynolds stresses, Journal of Physics: Conference Series, 3016, 012 033, 2025.

Frandsen, S., Barthelmie, R., Pryor, S., Rathmann, O., Larsen, S., Højstrup, J., and Thøgersen, M.: Analytical modelling of wind speed deficit in large offshore wind farms, Wind Energy, 9, 39–53, 2006.

Garrett, C. and Cummins, P.: The efficiency of a turbine in a tidal channel, Journal of Fluid Mechanics, 588, 243–251, 2007.

Gunn, K.: Improvements to the Eddy Viscosity Wind Turbine Wake Model, Journal of Physics: Conference Series, 1222, 012 003, 2019.

Jensen, N. O.: A note on wind generator interaction, Tech. Rep. Risø-M-2411, 2411, 1983.

Krantz, S. G. and Parks, H. R.: The implicit function theorem: history, theory, and applications, Springer Science & Business Media, 2002.

Lissaman, P. B.: Energy effectiveness of arbitrary arrays of wind turbines, Journal of Energy, 3, 323–328, 1979.

Luzzatto-Fegiz, P.: A one-parameter model for turbine wakes from the entrainment hypothesis, Journal of Physics: Conference Series, 1037, 072 019, 2018.

Mikkelsen, R.: Actuator disc methods applied to wind turbines, Ph.D. thesis, Technical University of Denmark, 2003.

Neunaber, I., Hölling, M., and Obligado, M.: Leading effect for wind turbine wake models, Renewable Energy, 223, 119 935, 2024.

Niayifar, A. and Porté-Agel, F.: Analytical modeling of wind farms: A new approach for power prediction, Energies, 9, 741, 2016.

Nishino, T. and Draper, S.: Local blockage effect for wind turbines, Journal of Physics: Conference Series, 625, 012 010, 2015.

Nishino, T. and Willden, R. H.: The efficiency of tidal fences: A brief review and further discussion on the effect of wake mixing, 32nd International Conference on Ocean, Offshore and Arctic Engineering, OMAE2013-10207, 2013.

Pope, S. B.: Turbulent flows, Cambridge University Press, 2000.

Qian, G.-W. and Ishihara, T.: A new analytical wake model for yawed wind turbines, Energies, 11, 665, 2018.

Shapiro, C. R., Starke, G. M., Meneveau, C., and Gayme, D. F.: A wake modeling paradigm for wind farm design and control, Energies, 12, 2956, 2019.

Sørensen, J. N., Mikkelsen, R., Sarmast, S., Ivanell, S., and Henningson, D.: Determination of wind turbine near-wake length based on stability analysis, Journal of Physics: Conference series, 524, 012 155, 2014.

Sørensen, T., Thøgersen, M. L., Nielsen, P., and Jernesvej, N.: Adapting and calibration of existing wake models to meet the conditions inside offshore wind farms, EMD International A/S. Aalborg, 2008.

Svenning, E.: Implementation of an actuator disk in OpenFOAM, Chalmers University of Technology, 2010.

https://doi.org/10.5194/wes-2026-76
Preprint. Discussion started: 13 May 2026

Vahidi, D. and Porté-Agel, F.: A new streamwise scaling for wind turbine wake modeling in the atmospheric boundary layer, Energies, 15, 9477, 2022a.

Vahidi, D. and Porté-Agel, F.: A physics-based model for wind turbine wake expansion in the atmospheric boundary layer, Journal of Fluid Mechanics, 943, A49, 2022b.

Van der Laan, M., Hansen, K. S., Sørensen, N. N., and Réthoré, P.-E.: Predicting wind farm wake interaction with RANS: an investigation of the Coriolis force, Journal of Physics: Conference Series, 625, 012 026, 2015.

Vermeulen, P.: An experimental analysis of wind turbine wakes, in: 3rd International Symposium on Wind Energy Systems, pp. 431–450, 1980.